AGU PUBLICATIONS

JGR

Journal of Geophysical Research: Solid Earth

RESEARCH ARTICLE
10.1002/2016JB013310

Key Points:
- Higher-resolution seismic image of the upper mantle beneath the Alpine and Apenninic region
- Continuity of slabs ruling out the hypothesis of slab break off in the study area
- Pinpoints for analysis of Cenozoic magmatism, (U)HP metamorphism, and Alpine topography

Supporting Information:
- Supporting Information S1

Correspondence to:
L. Zhao and M. G. Malusà,
zhaoliang@mail.iggcas.ac.cn;
marco.malusa@unimib.it

Citation:
Zhao, L., et al. (2016), Continuity of the Alpine slab unraveled by high-resolution *P* wave tomography, *J. Geophys. Res. Solid Earth*, *121*, doi:10.1002/2016JB013310.

Received 25 JUN 2016
Accepted 9 NOV 2016
Accepted article online 12 NOV 2016

Continuity of the Alpine slab unraveled by high-resolution *P* wave tomography

Liang Zhao[1,2], Anne Paul[3], Marco G. Malusà[4], Xiaobing Xu[1], Tianyu Zheng[1], Stefano Solarino[5], Stéphane Guillot[3], Stéphane Schwartz[3], Thierry Dumont[3], Simone Salimbeni[6], Coralie Aubert[3], Silvia Pondrelli[6], Qingchen Wang[1], and Rixiang Zhu[1]

[1]State Key Laboratory of Lithospheric Evolution, Institute of Geology and Geophysics, Chinese Academy of Sciences, Beijing, China, [2]CAS Center for Excellence in Tibetan Plateau Earth Sciences, Beijing, China, [3]ISTerre, University of Grenoble Alpes, CNRS, Grenoble, France, [4]Department of Earth and Environmental Sciences, University of Milano-Bicocca, Milan, Italy, [5]Istituto Nazionale di Geofisica e Vulcanologia, CNT, Genoa, Italy, [6]Istituto Nazionale di Geofisica e Vulcanologia, Bologna, Italy

Abstract The question of lateral and/or vertical continuity of subducted slabs in active orogens is a hot topic partly due to poorly resolved tomographic data. The complex slab structure beneath the Alpine region is only partly resolved by available geophysical data, leaving many geological and geodynamical issues widely open. Based upon a finite-frequency kernel method, we present a new high-resolution tomography model using *P* wave data from 527 broadband seismic stations, both from permanent networks and temporary experiments. This model provides an improved image of the slab structure in the Alpine region and fundamental pinpoints for the analysis of Cenozoic magmatism, (U)HP metamorphism, and Alpine topography. Our results document the lateral continuity of the European slab from the Western Alps to the central Alps, and the downdip slab continuity beneath the central Alps, ruling out the hypothesis of slab break off to explain Cenozoic Alpine magmatism. A low-velocity anomaly is observed in the upper mantle beneath the core of the Western Alps, pointing to dynamic topography effects. A NE dipping Adriatic slab, consistent with Dinaric subduction, is possibly observed beneath the Eastern Alps, whereas the laterally continuous Adriatic slab of the Northern Apennines shows major gaps at the boundary with the Southern Apennines and becomes near vertical in the Alps-Apennines transition zone. Tear faults accommodating opposite-dipping subductions during Alpine convergence may represent reactivated lithospheric faults inherited from Tethyan extension. Our results suggest that the interpretations of previous tomography results that include successive slab break offs along the Alpine-Zagros-Himalaya orogenic belt might be proficiently reconsidered.

1. Introduction

Along the Alpine-Zagros-Himalayan orogenic system, seismic tomography of the mantle reveals more or less discontinuous *P* wave velocity anomalies interpreted as the seismic signature of subducted lithospheric slabs [e.g., *Wortel and Spakman*, 2000; *Piromallo and Faccenna*, 2004; *Replumaz et al*., 2004]. It is generally accepted that these anomalies reflect the subduction of the large Tethyan realm and the subsequent collision of Africa, Arabia, and India with Eurasia [e.g., *Hafkenscheid et al*., 2006; *Capitanio et al*., 2010]. However, interpretations in terms of lateral and/or vertical slab continuities, length of the subducted slabs, and their relationship with geodynamic processes strongly depend on the resolution of the seismic tomography. This question is particularly crucial in the western part of the Tethyan orogenic system where the complex plate boundary area between Africa and Europe includes several microplates (e.g., Adria and Iberia) and orogenic belts that correspond to different subduction zones, in particular the Alps, Apennines, Betics, Dinarides, and Pyrénées (see Figures 1a and 1b) [*Jolivet and Faccenna*, 2000; *Vignaroli et al*., 2008; *Handy et al*., 2010; *Carminati et al*., 2012; *Malusà et al*., 2015]. In the Alpine region, two major and possibly interacting slabs have been recognized by geophysical investigations [*Kissling*, 1993; *Spakman et al*., 1993; *Solarino et al*., 1996; *Piromallo and Morelli*, 2003; *Lippitsch et al*., 2003; *Kissling et al*., 2006; *Giacomuzzi et al*., 2011]. They are the SE dipping European (Alpine) slab to the north and the west dipping Adriatic (Apenninic) slab to the south. Although surface geology data suggest that the main Alpine and Apenninic structures may be persistent along strike (Figure 1a), the lateral and downdip continuity of these slabs is not fully resolved, possibly due to uneven distribution of seismic stations. Available *P* wave tomography models show evident but discontinuous high-

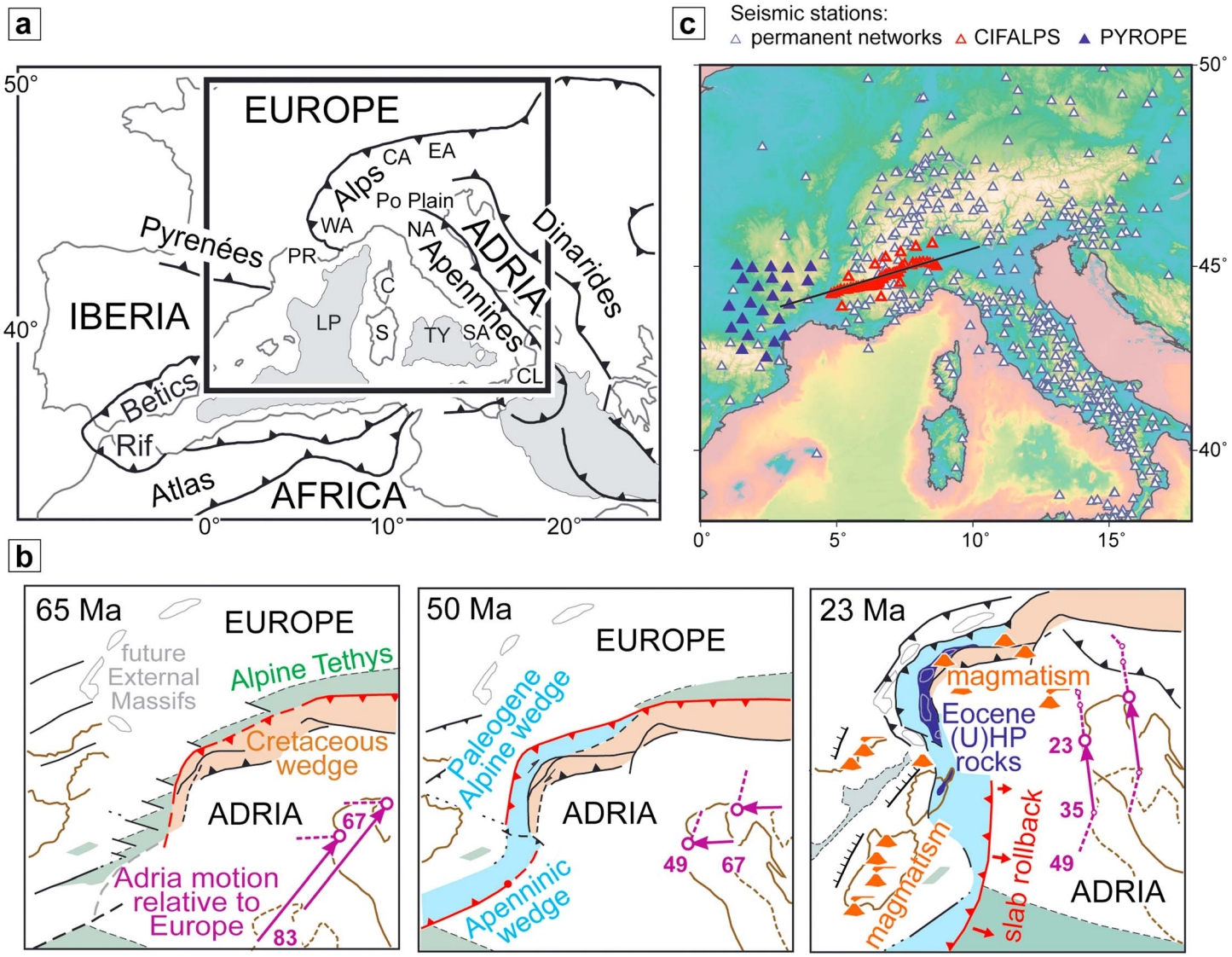

Figure 1. (a) Tectonic sketch map of the study area. C: Corsica; CA: central Alps; CL: Calabria: EA: Eastern Alps; LP: Ligurian-Provençal basin; NA: Northern Apennines; PR: Provence; S: Sardinia; SA: Southern Apennines; TY: Tyrrhenian basin; and WA: Western Alps. The black box indicates the area of frame C. (b) Cenozoic evolution of Alpine and Apenninic subductions and coeval magmatism, simplified after *Malusà et al.* [2015, 2016b]. In red are active subduction zones; purple arrows indicate Adria trajectories relative to Europe [from *Dewey et al.*, 1989] (numbers = age in Ma). (c) Location map of seismic stations used to construct the tomographic images from permanent networks (open gray triangles) and CIFALPS (open red triangles) and PYROPE (blue triangles) temporary arrays. The solid line gives the location of the cross section shown in Figure 4.

velocity anomalies associated with the Alpine and Apenninic subduction zones [*Lucente et al.*, 1999; *Lippitsch et al.*, 2003; *Piromallo and Morelli*, 2003; *Giacomuzzi et al.*, 2011], as well as high-velocity anomalies in areas where no slab is expected according to geological evidence (e.g., the Provençal margin of SE France) [*Piromallo and Morelli*, 2003]. Due to such uncertainties, the slab structure in the transition zone between the Alps and the Apennines is still largely unknown, and it is not clear whether the subduction beneath the Eastern Alps is directed southward [e.g., *Piromallo and Faccenna*, 2004; *Spakman and Wortel*, 2004] or northward [*Lippitsch et al.*, 2003]. The downdip slab continuity beneath the Western Alps and the central Alps is also debated, with major gaps possibly supportive of slab break off [*Lippitsch et al.*, 2003; *Spakman and Wortel*, 2004; *Kissling et al.*, 2006] that conflict with the more continuous and apparently steeper slab alternatively imaged beneath the Western Alps [e.g., *Piromallo and Faccenna*, 2004].

The steepness and downdip continuity of the Alpine slab, and its possible interaction with the Apenninic slab to the south [e.g., *Vignaroli et al.*, 2008; *Malusà et al.*, 2016a], have major implications for (U)HP

metamorphism, magmatism, and relief development in the Alpine region during the Cenozoic [*von Blanckenburg and Davies*, 1995; *Guillot et al*., 2009; *Lustrino et al*., 2011; *Faccenna et al*., 2014; *Fox et al*., 2015]. However, uncertainty in both Alpine and Apenninic slab structures leaves many questions widely open, both concerning the peculiar Cenozoic magmatism in the Alps, which is classically ascribed to slab break off [e.g., *von Blanckenburg and Davies*, 1995; *Dal Piaz et al*., 2003], and the very low paleogeothermal gradients documented during Alpine subduction, but unexpected in areas characterized by very slow convergence [*Malusà et al*., 2015].

In this article, we present new high-resolution tomography images of the Alpine region in order to better constrain not only the structure of the Alpine and Apenninic slabs but also their complex transition along strike. Implications for Alpine magmatism, (U)HP metamorphism, and relief development in the western part of the Tethyan orogenic system are eventually discussed.

2. Tectonic Setting

The Alps-Apennines orogenic belt is the result of the progressive closure of the Tethyan Ocean in between the Adriatic and European passive margins since the Mesozoic [e.g., *Handy et al*., 2010, and references therein]. Meso-Cenozoic Adria-Europe convergence was chiefly accommodated by subduction along a complex paleotrench, showing a major right-angle bend between the central Alps and the Western Alps and a NE-SW trend along the future Provençal margin (Figure 1b). Such a paleotrench was strongly oblique both relative to Adria motion [e.g., *Dewey et al*., 1989] and relative to the European paleomargin of the Tethys [e.g., *Malusà et al*., 2016b]. Adria represented the upper plate of the subduction system in the central Alps and Western Alps and the lower plate in the Apennines [*Jolivet and Faccenna*, 2000; *Vignaroli et al*., 2008; *Malusà et al*., 2015]. After the accretion of extensional allochthons originally belonging to the Adriatic margin, most of the Tethyan Ocean was subducted beneath the Adriatic microplate in Cretaceous times, during NE-SW convergence between Adria and Europe [*Dewey et al*., 1989; *Zanchetta et al*., 2015]. The slow E-W convergence documented along this plate boundary in Paleocene-early Eocene times was instead accommodated by two opposite-dipping subduction zones, an eastward (Alpine) subduction that was active from the Western Alps to Corsica, bringing European continental crust down to (U)HP depth [e.g., *Rubatto and Hermann*, 2001] and a coeval northwestward subduction that was active in the future Apennines (Figure 1b). Paleogeothermal gradients during subduction were extremely low, especially in the Alpine trench (4–6°C/km) [*Malusà et al*., 2015], where subduction was choked in middle-late Eocene times by the arrival of thick European crust at the trench, and (U)HP rocks were rapidly exhumed at the surface as soon as the Adriatic Plate started moving toward the NNE (Figure 1b). The Adriatic slab thus obliquely subducted beneath Corsica and reached the remnants of the Alpine orogenic wedge by the end of the Oligocene [*Malusà et al*., 2016b]. However, it is not clear whether the Adriatic slab moved farther north in the Neogene, when the Adriatic trench began retreating toward the east, leading to the opening of the Ligurian-Provençal basin [*Jolivet and Faccenna*, 2000; *Malusà et al*., 2016a] and controlling the counterclockwise rotation of Corsica-Sardinia and the progressive migration of Apenninic magmatism [*Lustrino et al*., 2011]. During Adriatic trench retreat, the uppermost levels of the Alpine orogenic wedge also experienced major counterclockwise rotations along the transition zone with the Apennines [*Maffione et al*., 2008], but the effects of such rotations on the deepest segments of the Alpine slab are still unknown.

Because of slab rollback, the amount of subduction was certainly greater in the Apennines than in the Alps [*Piromallo and Faccenna*, 2004], where any causal relationship between the observed magmatic climax at ~30 Ma [*Lustrino et al*., 2011] and the inferred break off of the Tethyan slab [e.g., *Davies and von Blanckenburg*, 1995] is still unproven. The amount of subduction in the central Alps was on the order of 450 km [*Malusà et al*., 2015], whereas it progressively increased along the Apenninic trench from the north toward the south, reaching ~1300 km in Calabria [*Piromallo and Morelli*, 2003].

3. Data and Imaging

3.1. Data Selection and Analysis

This study used data collected from 527 broadband seismic stations, benefiting from recent opening of European seismic databases, improvement of permanent broadband network, and consequent improvement of data quality. Among these stations, 449 were from several permanent networks distributed by the

European Integrated Data Archive (EIDA) European archive (http://webdc.eu/webdc3/; open gray triangles in Figure 1c), 23 were from the PYROPE experiment [*Chevrot et al*., 2014] (blue triangles in Figure 1c), and 55 are from the CIFALPS experiment [*Zhao et al*., 2015] (red triangles in Figure 1c). CIFALPS (i.e., China-Italy-France Alps Seismic Survey) was a passive seismic transect operated from July 2012 to September 2013, which cross-cuts the entire Western Alps (Figure 1c). For the PYROPE experiment, we used data for the time period overlapping with the CIFALPS experiment, whereas for the permanent stations we selected data from July 2012 to November 2014. As a result, our study is based on a much greater number of stations and a much denser coverage than any previous work, in particular in the Western Alps [e.g., *Lippitsch et al*., 2003; *Piromallo and Morelli*, 2003; *Giacomuzzi et al*., 2011].

In total, 199 events with epicentral distances ranging between 30° and 110° from the study area and minimum moment magnitude of 5.8 were selected for traveltime tomography (see supporting information Figure S1). The azimuthal coverage is not uniform mainly due to a limited number of events in the southern quadrant. In order to reduce the influence of this uneven distribution, we selected only events with the best signal-to-noise ratio in the ranges of back azimuth with very dense coverage. The resulting coverage is sufficient to provide the best ray crisscrossing given the limitations from the southern quadrant and ensures a fairly uniform resolution in the upper mantle of the study area.

Traveltime delays are frequency dependent due to wavefront healing and diffraction of seismic waves [e.g., *Hung et al*., 2004]. To take advantage of changes in the sensitivity of *P* waves with frequency, we measured relative delay times in four frequency bands, 0.02–0.1 Hz, 0.1–0.8 Hz, 0.4–0.8 Hz, and 0.8–2.0 Hz. Since we aimed at retrieving high-resolution features, we inverted traveltime residuals measured in the shortest period ranges (0.4–0.8 Hz and 0.8–2 Hz) that correspond to wavelengths of the order of or smaller than our grid spacing of 25 km (shown in Figure 2a). The two long-period bands (0.02–0.1 Hz and 0.1–0.8 Hz) were used to guarantee the highest quality of readings, as explained below.

We measured relative time residuals using the multichannel cross-correlation technique (MCCCT) [*Vandecar and Crosson*, 1990] on vertical component records. As the study region is broad and teleseismic traveltime differences may be as large as a few seconds due to very heterogeneous crustal and mantle structures [e.g., *Lippitsch et al*., 2003; *Giacomuzzi et al*., 2011], automatic picking using the MCCCT in time windows computed from a standard Earth model is prone to errors including cycle skipping. Potential cycle skipping problems are even stronger in the targeted high-frequency bands. To avoid such problems, we first picked the *P* wave onset manually on each single record by visually comparing and aligning the *P* waveforms filtered in the 0.1–1 Hz frequency band. In a second step, the differential traveltimes were retrieved by the MCCCT in time windows positioned on the manual picks and from signals filtered in the four frequency bands (0.02–0.1 Hz, 0.1–0.8 Hz, 0.4–0.8 Hz, and 0.8–2.0 Hz). We started processing the low-frequency band and moved on to higher frequencies because low frequencies are less prone to cycle skipping. For each single event we selected only stations with average correlation coefficient (average of the maxima of the correlation functions with all other stations) larger than 0.8 in the four frequency bands. We visually checked all the waveforms and the correlation functions and compared them in all frequency bands to further guarantee the quality of our data set. Supporting information Figure S2 shows examples of vertical component records aligned on the traveltime readings in the 0.4–0.8 Hz band for two events with different signal-to-noise ratios.

In the final step of data selection, we kept only the highest-quality residuals (average correlation coefficient ≥ 0.85) measured in the two short-period ranges (0.4–0.8 Hz and 0.8–2 Hz). The final data set included 41,838 relative traveltime residuals (27,650 in the 0.4–0.8 Hz band and 14,188 in the 0.8–2 Hz band) with a variance of 0.38 s^2. The average number of readings for a single event in the 0.4–0.8 Hz band is 139, with a minimum of 14 and a maximum of 359. Based on comparisons with relative delay times measured by a different method on a trial subset of events [*Chevrot*, 2002], we estimated that the average uncertainty on our data is <0.1 s.

Supporting information Figure S3 shows examples of relative traveltime residuals measured in the 0.4–0.8 Hz band at stations in the Western Alps for four events with east, SSE, WSW, and NNW back azimuths. The residuals are very coherent at neighboring stations, with positive residuals (late arrivals) in the Southeast basin (France) and the Po Plain and negative residuals (early arrivals) at the boundary between the Western Alps and the Po Plain. The variations in residuals are stronger for events 1 and 2 with east and SSE back azimuths, which suggests that wavefronts incoming from the west travel across more homogeneous structures than wavefronts incoming from the east.

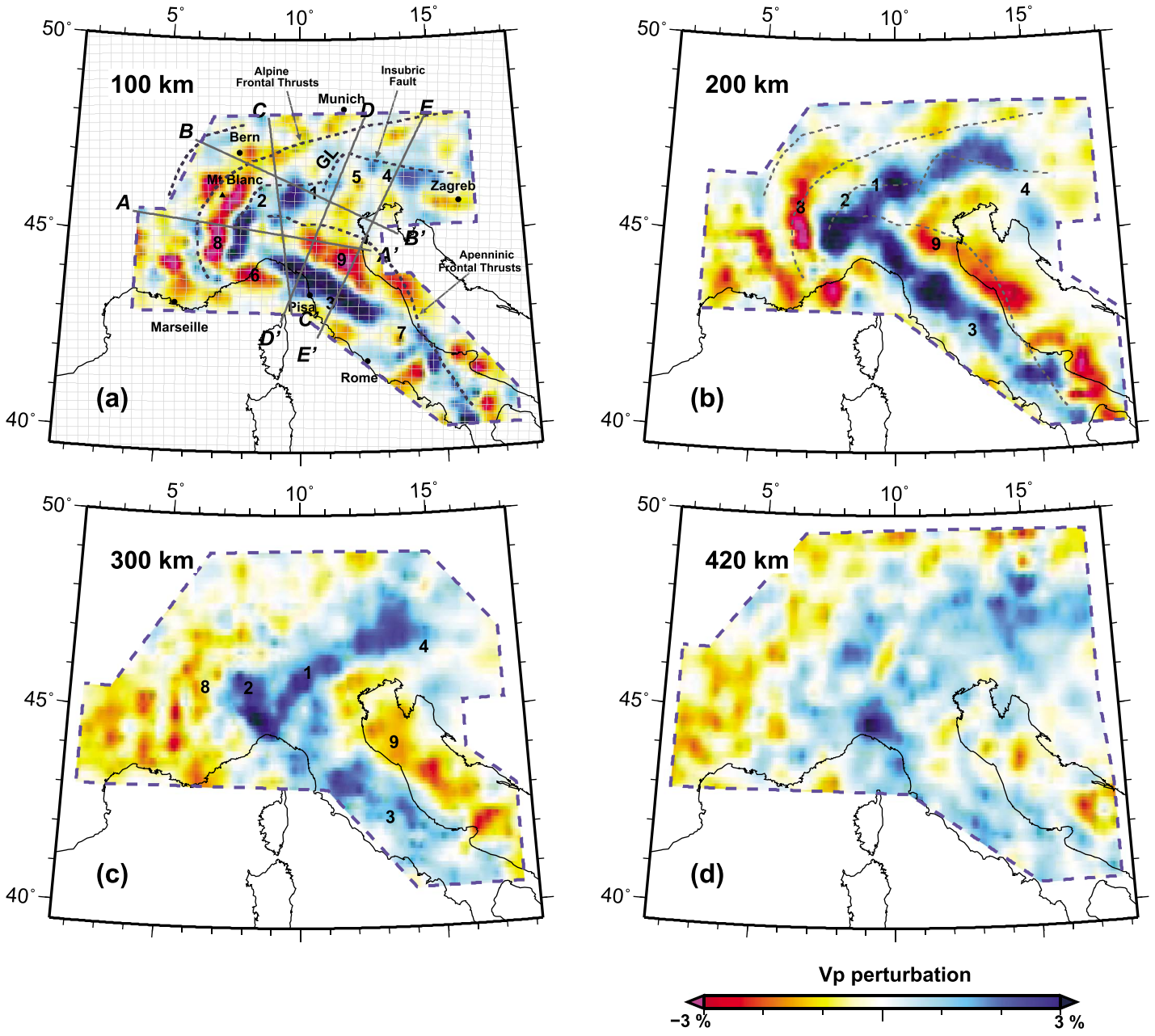

Figure 2. Upper mantle depth slices in the *P* wave velocity perturbation model resulting from our finite-frequency tomography (traveltimes corrected for crustal propagation in the EPcrust model) [*Molinari and Morelli*, 2011]. The blue dashed lines mark the outlines of the well-resolved areas estimated from resolution tests (supporting information Figures S9, S11, and S12). Note the lateral continuity of the Alpine and Apenninic slabs at 200 km depth. The black short dashed lines in Figure 2a indicate the main tectonic boundaries; the gray solid lines show the locations of the cross sections displayed in Figure 3; the gray grid lines in Figure 2a show the grid points used in the inversion. GL: Giudicarie Line; 1 to 4: high-velocity anomalies (1, central Alps slab; 2, Western Alps slab; 3, Northern Apennines slab; and 4, Dinaric slab); 5 to 7: major gaps; 8 and 9: low-velocity anomalies (see text for details).

To avoid contamination of upper mantle tomography by crustal anomalies, we corrected residuals for traveltimes within the crust. This correction is potentially important in the Alpine region because of changes in crustal thickness and strong crustal heterogeneities including thick sedimentary basins and a high-velocity mantle slice at shallow depth in the Western Alps [*Lippitsch et al.*, 2003; *Waldhauser et al.*, 2002]. We calculated traveltime corrections by using the EPcrust reference model [*Molinari and Morelli*, 2011] and assuming vertically incident plane waves. Supporting information Figure S4 shows comparisons of relative time residuals before and after crustal correction for stations along the CIFALPS profile, for the same four events as Figure S3 and in the 0.4–

0.8 Hz band. The corrections are >1 s because the profile crosses two basins (the Southeast basin of France in the west and the Po Plain in the east) and the high-velocity Ivrea body (at 7.5–8°E). They, however, do not strongly alter the shape of the residual curves, which are characterized by large and rapid changes. Including crustal corrections improves the variance reduction by 4% (see section 3.2), but it induces only slight differences in the final velocity perturbation model at depths ≥ 100 km (see supporting information Figure S5). All the results presented below were computed with residuals corrected for crustal propagation.

We are aware that our crustal corrections have two drawbacks. First, the EPcrust model is an oversimplification of the actual heterogeneity of the Alpine crust. For example, it does not include all the details of the latest Moho map of the area published by *Spada et al*. [2013], including a deep Moho trough in the Northern Apennines. EPcrust is, however, the latest crustal model publicly available to date that covers the whole study area. The second drawback is that we neglected the effect of 3-D propagation in the heterogeneous crust of nonvertical rays from different azimuths [*Waldhauser et al*., 2002]. In spite of these drawbacks, a synthetic test demonstrates that our tomography results are not significantly affected by smearing of crustal anomalies to mantle depth (see section 5.5, Figure 6, and supporting information Figure S15).

3.2. Imaging Methodology

The tomographic model space is a 1600 km × 1600 km area centered at 8°E/45°N that extends to 1500 km depth. The volume is parameterized within a grid of regular nodes with 26.6 km × 24.3 km × 25 km spacing (N-S, E-W, *z*; Figure 2a). We used the *P* wave data set to construct inversion equations based on a finite-frequency kernel formulation [*Dahlen et al*., 2000; *Hung et al*., 2000, 2004]. A damped LSQR (Sparse Equations and Least Squares) algorithm [*Paige and Saunders*, 1982] was applied to invert the matrix. The damping parameters were empirically determined based on the trade-off between model norm and variance reduction (see supporting information Figure S6). The models discussed in this paper are built using damping parameters that yield a 74% reduction of the variance on *P* wave time residuals that is a final variance of 0.11 s^2.

4. Large-Scale Features of the *P* Wave Model

We first present the major features of our 3-D tomography model (Figures 2 and 3 and supporting information Figure S7). Resolution tests specifically designed to demonstrate the quality of our images are discussed in section 5.

Unlike previous tomography models [e.g., *Lippitsch et al*., 2003; *Piromallo and Morelli*, 2003; *Giacomuzzi et al*., 2011], the most salient feature of the new model is the continuity of the subducted slabs at depths ≥180 km. Figures 2 and 3 document the following: (1) the downdip continuity of the European slab beneath the central Alps (1 in Figure 3c), (2) the lateral continuity of the European slab from the central Alps to the Western Alps (1 and 2 in Figure 2), and (3) the lateral continuity of the Adriatic slab in the Northern Apennines (3 in Figure 2). Supporting information Figure S7 documents the progressive merging of high-velocity anomalies with increasing depth from 100 km to 200 km.

The European slab has a steep southeastward dip in the central Alps (1 in Figures 3b and 3c). In the Western Alps (2 in Figure 3a), the amplitude of the high-velocity anomaly is stronger than in the central Alps. The complex high-velocity anomaly observed in cross-section A-A′ at depth ≥150 km probably reflects a combined effect of the Western Alps and central Alps slabs (Figure 3a). Along the CIFALPS profile where the station density is high (5–10 km spacing), the high-velocity anomaly is continuous from the uppermost mantle where it links with the subducted European crust recognized by receiver function imaging [*Zhao et al*., 2015] (Figure 4). A strong low-velocity anomaly is observed at 100–250 km depth in the upper mantle of the Western Alps, which does not extend to the central Alps east of 8°E (8 in Figure 2; see also Figure 4). Another low-velocity anomaly is observed beneath the Po Plain in the Adriatic uppermost mantle (9 in Figures 2 and 3), between the central Alps and the Northern Apennines slabs.

When observed in map view, the high-velocity anomaly associated with the Alpine subduction is continuous along strike from the southernmost Western Alps to the easternmost central Alps at depths ≥180 km (Figures 2b, 2c, and S7). The European slab is recognized immediately to the west of the Giudicarie Line (GL in Figure 2a) on the 100 km depth slice (1 in Figure 2), but it is not observed farther east. Instead, a NW-SE trending high-velocity anomaly is detected beneath the Eastern Alps (4 in Figure 2), with an angle of 30° to 60° (depending on the depth range) relative to the strike of the Alpine frontal thrusts (dotted line in

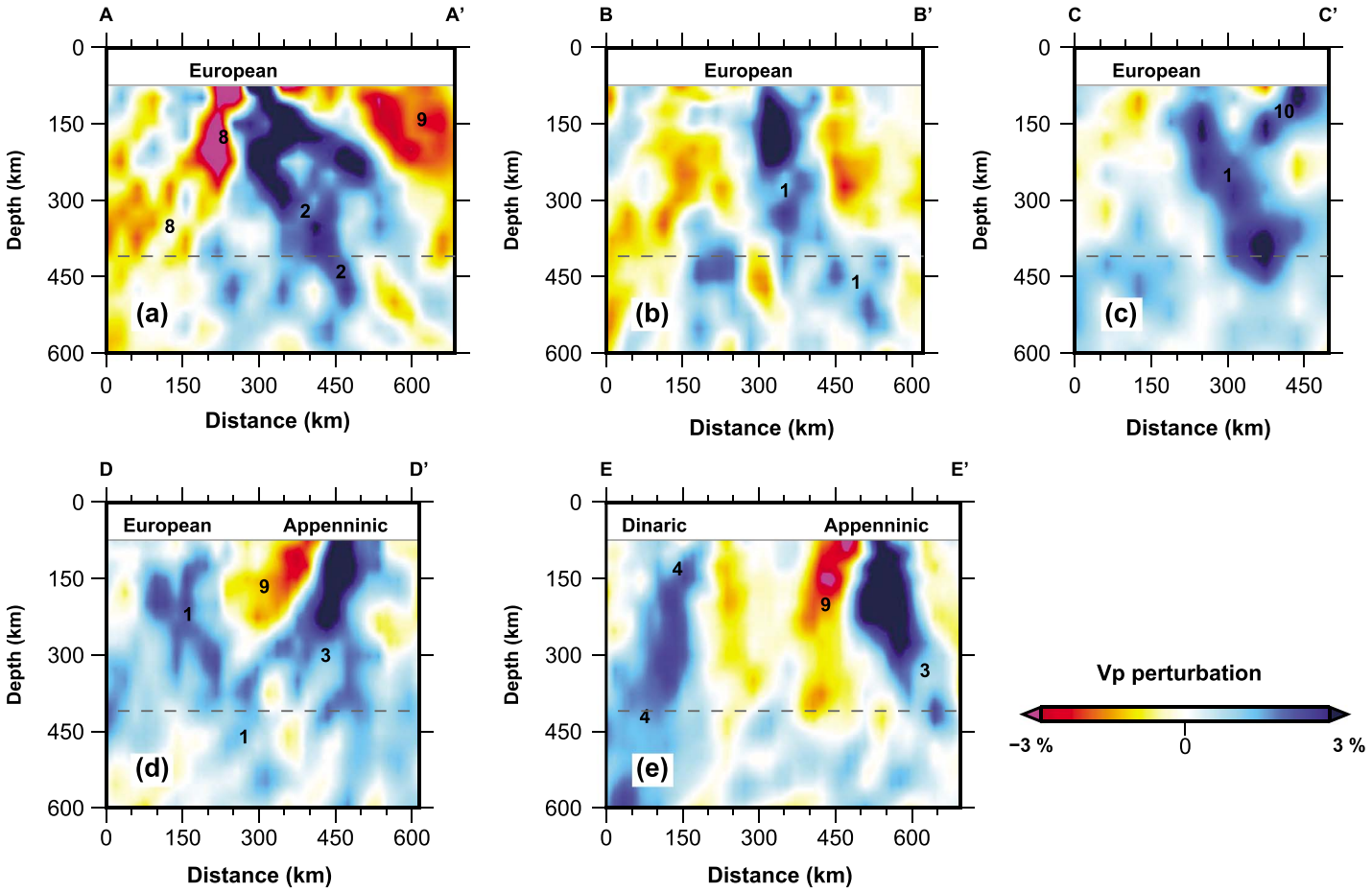

Figure 3. Cross sections in our V_P perturbation model. The locations of the cross sections are shown in Figure 2a. The labels on top of the sections are slab names. (a, b) Note the downdip continuity of the Alpine (European) slab beneath the Western Alps and central Alps. 1 to 9: same keys as in Figure 2; 10: north dipping high-velocity anomaly beneath the Alps-Apennines transition zone (see text for details).

Figure 2a). At 100 km depth, the boundary between the south dipping slab beneath the central Alps (1 in Figures 2 and 3) and the north dipping slab beneath the Eastern Alps (4 in Figures 2 and 3e) is marked by an evident step (5 in Figure 2a) located beneath the Giudicarie Line.

In the southern part of the model, the Apenninic slab (3 in Figure 3e) is steeply dipping to the SW beneath the northern Tyrrhenian Sea. By contrast, the Apenninic slab close to the Alps-Apennines transition zone is near vertical (3 in Figure 3d). Along the Alps-Apennines transition zone, a small north dipping high-velocity anomaly (10 in Figure 3c) is located at depth $<$200 km above the central Alps slab (1 in Figure 3c), and a gap between this north dipping high-velocity anomaly and the Western Alps slab can be observed in map view (6 in Figure 2a). To the south, the high-velocity anomaly of the Apenninic slab is continuous along strike (Figure 2b and supporting information Figure S7), except at shallow depth ($\leq$160 km) where a major gap (7 in Figure 2a) is observed north of Rome, at the transition between the Northern and the Southern Apennines. This continuity of the northern Apenninic slab was already mentioned by *Giacomuzzi et al.* [2011] for depths $\geq$140 km.

The continuity of the high-velocity slabs unraveled by our tomography below 180 km depth is a major difference compared to previous works. The two tomographies by *Lippitsch et al.* [2003] and *Piromallo and Morelli* [2003] showed discontinuous high-velocity anomalies with gaps larger than 100 km that were interpreted as indications for slab break off. In order to provide conclusive evidence on the slab continuity and demonstrate that gaps of size $>$100 km could not be missed by our tomography, we performed a series of specifically designed resolution tests.

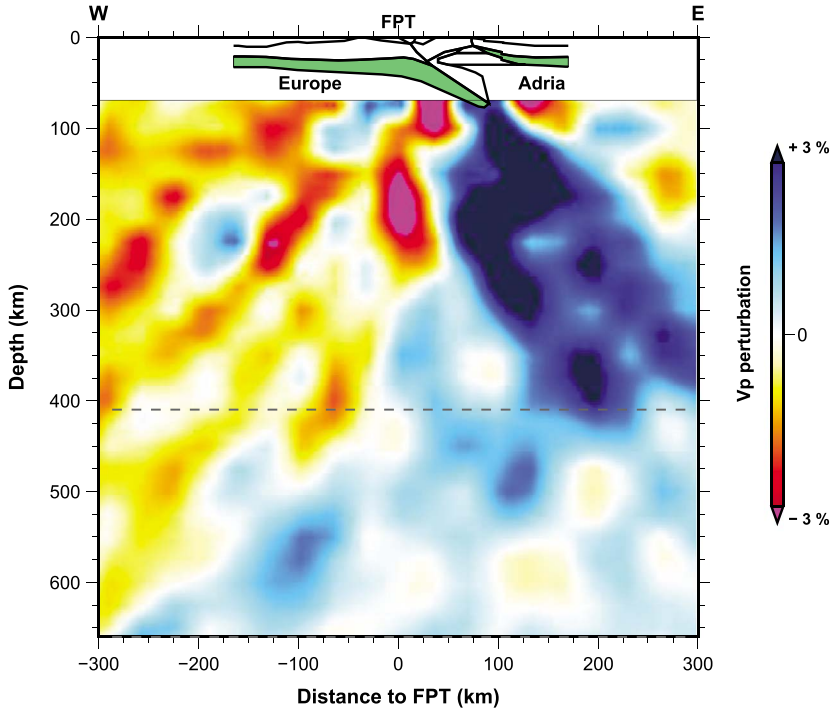

Figure 4. Cross section of V_P perturbations along the CIFALPS profile (location shown in Figure 1c). The crustal model estimated by *Zhao et al*. [2015] from receiver function imaging complemented with gravity modeling and geological data is shown in the upper part, with green color representing the lower crust. FPT: Frontal Penninic Thrust.

5. Resolution Tests

Synthetic 3-D velocity models were designed and used to generate synthetic traveltime delays for the same event-receiver distribution as in the original data set. A 10% Gaussian white noise was added to the synthetic relative traveltime residuals to simulate noise, which exceeds the estimated uncertainty on the traveltime measurements. The synthetic data sets were then inverted using the same parameters as in the inversion of observed data.

5.1. Checkerboard Tests

We first conducted general checkerboard experiments with alternating high- and low-velocity anomalies of $\pm$4.5% $\delta \ln V_P$ within individual blocks of size $5 \times 5 \times 5$ grid cells (i.e., ~125 km $\times$ 125 km $\times$ 125 km) (supporting information Figure S8). The depth slices and cross sections in the recovered models are shown in the supporting information Figure S9. The test shows that the resolution is good to 700 km depth for anomalies with horizontal size $\geq$125 km, even with 10% noise in the data, provided that station coverage is dense enough. Inspection of the recovered images shows that the location and shape of the structures are fairly well rendered, although the recovered velocity anomalies are attenuated. We used this checkerboard test to define the part of the 3-D model that is sufficiently well resolved to be further discussed and interpreted (areas bordered by dashed lines in supporting information Figure S9). In order to remove any doubt on the resolution in specific areas (for example, in the northeastern corner), we crosschecked the results of the checkerboard test with other resolution tests.

5.2. Tests of the Continuity of High-Velocity Slabs

This series of tests were specifically designed to test how well the data set resolves the 3-D continuity of the high-velocity slab structures.

Considering that previous tomography studies detected low-velocity gaps with thickness >100 km in the high-velocity slabs beneath the Western Alps and the Apennines [*Lippitsch et al*., 2003; *Piromallo and Morelli*, 2003], we tested a synthetic model where low-velocity anomalies of 60 km thickness cut steeply

dipping cylinders of high velocity (input model displayed in the supporting information Figure S10). Cylinders have horizontal diameters from 100 to 160 km and velocity perturbations of $\pm 4\%$ $\delta \ln V_P$. Note that the European and Adriatic synthetic slabs dip in directions opposite to actual ones in order to check whether the uneven distribution of events may influence the apparent dip of the imaged slabs. The output of the inversion displayed in the supporting information Figure S11 shows that the locations and shapes of low-velocity gaps are fairly well rendered (supporting information Figures S11e and S11i), while high-velocity slabs with opposite-dipping directions are also well reconstructed. Depth sections D-D′ and E-E′ (supporting information Figures S11h and S11i) along profiles located at less than 125 km distance illustrate that horizontal smearing is negligible for both high- and low-velocity anomalies. This observation confirms that horizontal resolution is better than 125 km (in this area and in other areas with better or similar station coverage), which implies that the horizontal continuity of the high-velocity slabs observed in Figures 2 and 3 is well constrained.

5.3. Resolution Tests Along the CIFALPS Profile

We used many more stations than previous tomography studies, including the CIFALPS temporary linear array with dense spacing (5–10 km) that significantly improves the resolution in the Western Alps. The following series of resolution tests were designed to quantify the reliability of the tomography beneath the CIFALPS array.

The first test aimed at checking the reliability of the continuous high-velocity anomaly that extends from the deepest edge of the European crust [*Zhao et al*., 2015] down to the mantle transition zone. We built a new synthetic model based on our 3-D $\delta \ln V_P$ model where we replaced part of the high-velocity slab by a cylinder with low-velocity anomaly of -4% $\delta \ln V_P$ and horizontal diameter of 120 km extending from 80 to 140 km depth to mimic a possible slab break off beneath the CIFALPS profile (Figure 5a). The inversion result (Figure 5b) illustrates that such a slab break off would be recognized, even though the amplitude of the low-velocity anomaly is attenuated. We also tested other synthetic models with synthetic slab break offs at depths between 100 km and 250 km (upper boundary), which all show that the discontinuity is well probed by our tomography.

Our new model also shows a low-velocity body beneath the European side of the Western Alps (8 in Figures 2a, 2b, 3a, and 4). In order to test if the smearing effects exaggerate the size of the low-velocity volume, we set a cylinder with anomaly of +4% $\delta \ln V_P$ and horizontal diameter of 100 km extending from depth of 100 km to 150 km (Figure S12a). Figure S12b shows that the major features of the input high-velocity anomaly can be retrieved by the inversion.

5.4. Test of the Influence of the Frequency Bandwidth

To document the resolution improvement provided by the selection of the two highest-frequency bands (0.4–2 Hz), we show in the supporting information Figures S13 and S14 the result of the inversion of delay times measured in the four frequency bands (0.02–2 Hz). A comparison with Figures 2 and 3 shows that the models are overall similar except that velocity perturbations are slightly weaker in the 0.02–2 Hz inversion, in particular at depths $>$300 km. Indeed, *Maupin and Kolstrup* [2015] quantified this sensitivity reduction of long-period (20 s) relative delay times with depth and attributed them to the increase in diameter of absolute kernels with depth that lead to a smaller amplitude of the relative kernels. Conversely, they observed no sensitivity reduction at short period (2 s). The enhanced sensitivity of short-period delay times, in particular at large depth ($>$300 km), justifies our decision to invert them.

5.5. Tests of the Leakage of Crustal Heterogeneities to Mantle Depths

As discussed in section 3.1, a number of publications have argued that correction of traveltimes for propagation in a 3-D accurate model of the Alpine crust is required to avoid smearing of crustal anomalies to mantle depth [e.g., *Waldhauser et al*., 2002; *Lippitsch et al*., 2003]. Therefore, we designed the following series of tests to check whether the strong heterogeneities of the Alpine crust (deep foreland basins, thick crust, and high-velocity Ivrea body) may significantly deteriorate our results.

The Ivrea body has been recognized for a long time as a high-density (3000 kg m^{-3}), high-velocity body (7.4 km s^{-1}) located at upper crustal depth (top at 10 km depth) beneath the Western Alps [*Closs and Labrouste*, 1963]. Following the results of the local earthquake tomography by *Diehl et al*. [2009], we modeled

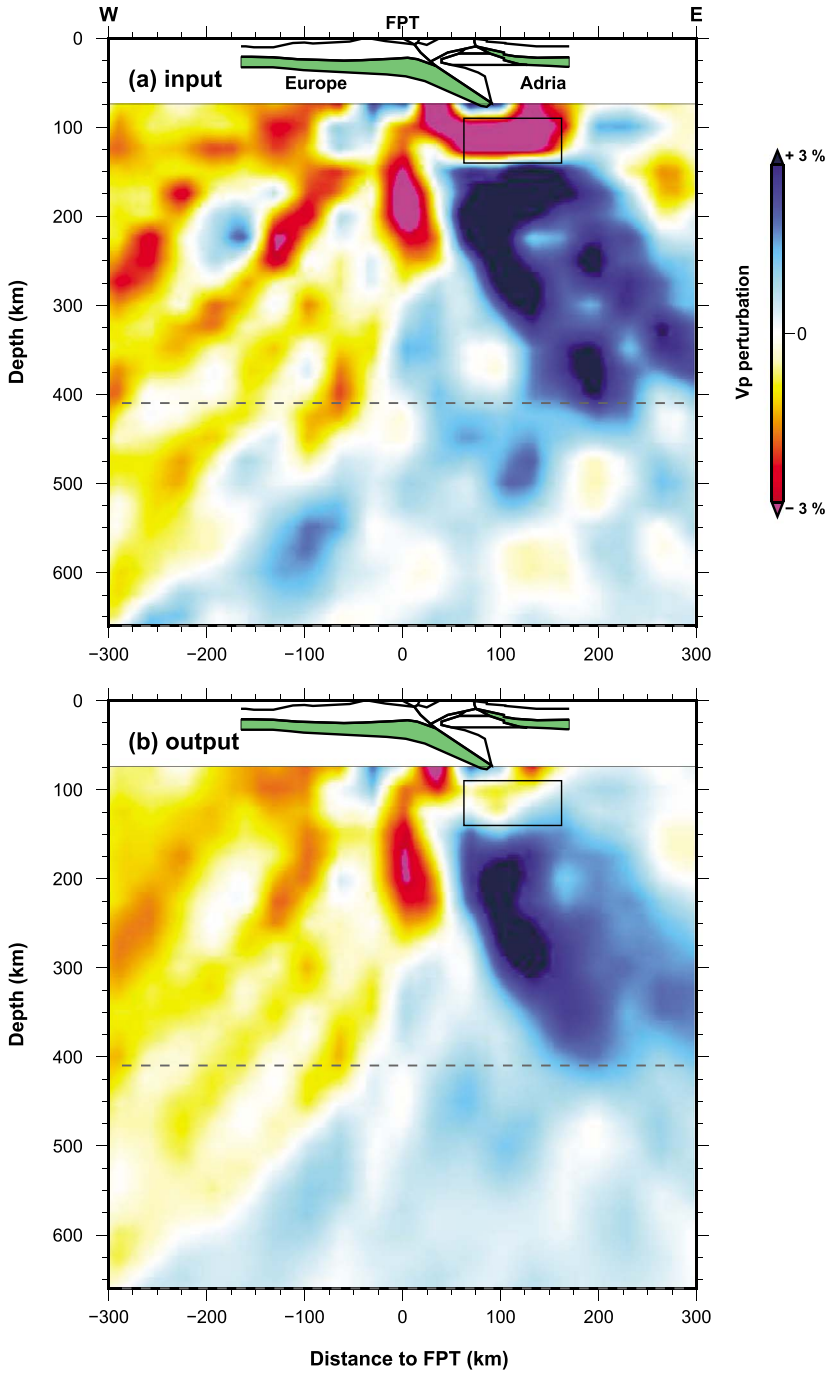

Figure 5. Resolution test of the continuity of the European slab along the CIFALPS profile in the Western Alps. (a) Input model obtained by substituting a cylinder volume in the final model of Figure 4 with a −4% velocity anomaly (rectangle). (b) Output model.

the body as an arc-like volume with strong anomaly of +25% $\delta \ln V_P$ extending from 10 km to 35 km depth (supporting information Figure S15). In order to test the effect of sedimentary basins, we also set strong low-velocity anomalies of −5% $\delta \ln V_P$ in the depth range 0–25 km (minimum thickness allowed by our grid size) that mimic the Po Plain, the Southeast basin of France, and the Molasse basin (supporting information Figure S15). Figure 6 shows the result of the inversion using the same inversion parameters as for observed time residuals. It documents that the leakage of crustal anomalies to upper mantle depth is weak. Figure 6

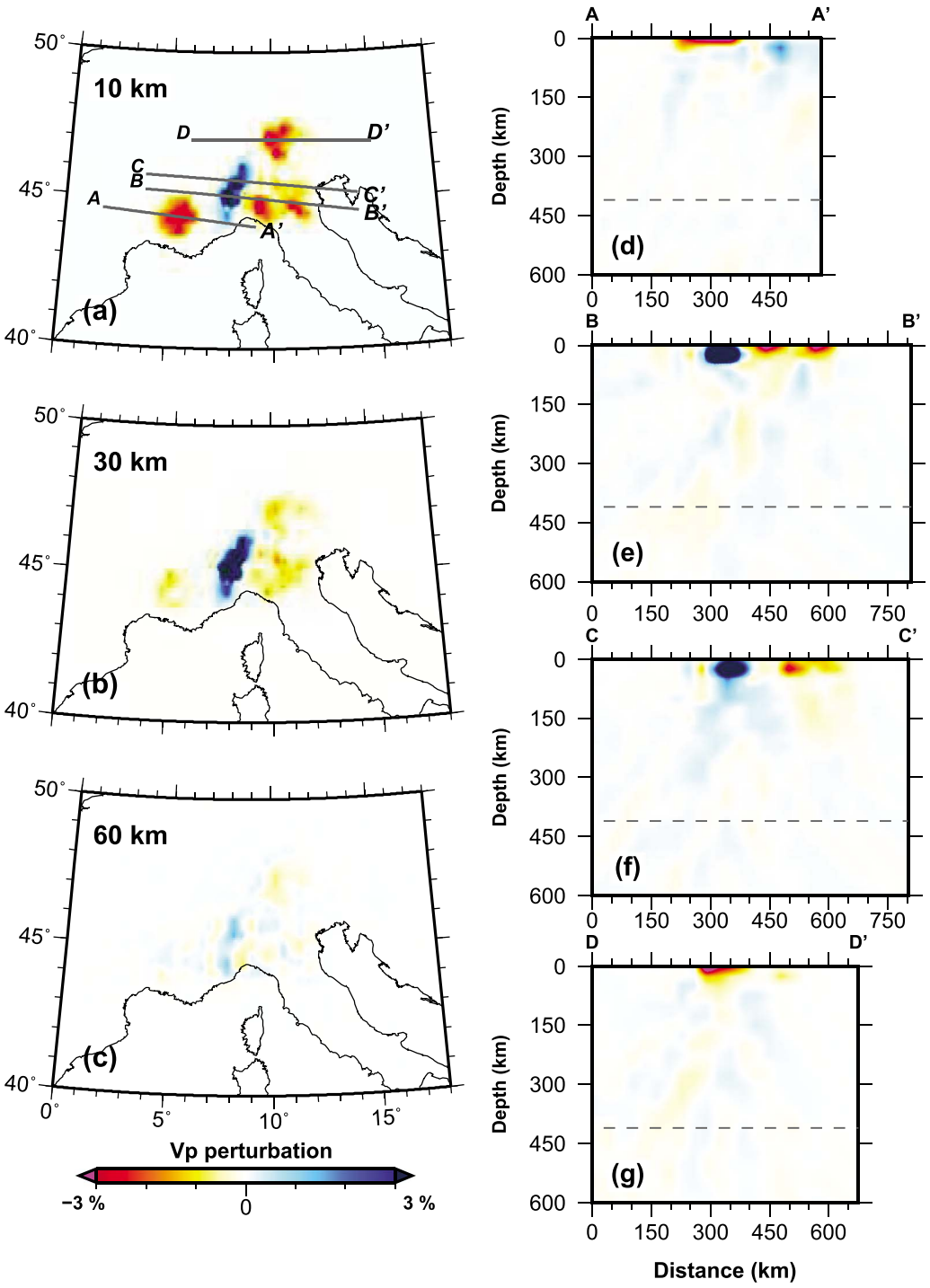

Figure 6. Results of a resolution test with velocity anomalies confined in the crust. The input model (displayed in supporting information Figure S15) has low-velocity anomalies of -5% $\delta \ln V_P$ in the depth range 0–25 km to mimic the sedimentary basins of the Po Plain, the Southeast basin of France, and the Molasse basin in Switzerland and southern Germany, and a high-velocity anomaly of +25% $\delta \ln V_P$ to mimic the Ivrea body. The leakage of shallow crustal anomalies to mantle depth is almost negligible.

illustrates in particular that the smearing to upper mantle depths of the strong anomaly simulating the Ivrea body has a negligible contribution to the high-velocity slab imaged beneath the Po Plain (for example, $<$0.5% at 150 km depth in cross-section C-C′, Figure 6f, as compared to $>$3.5% at the same depth in

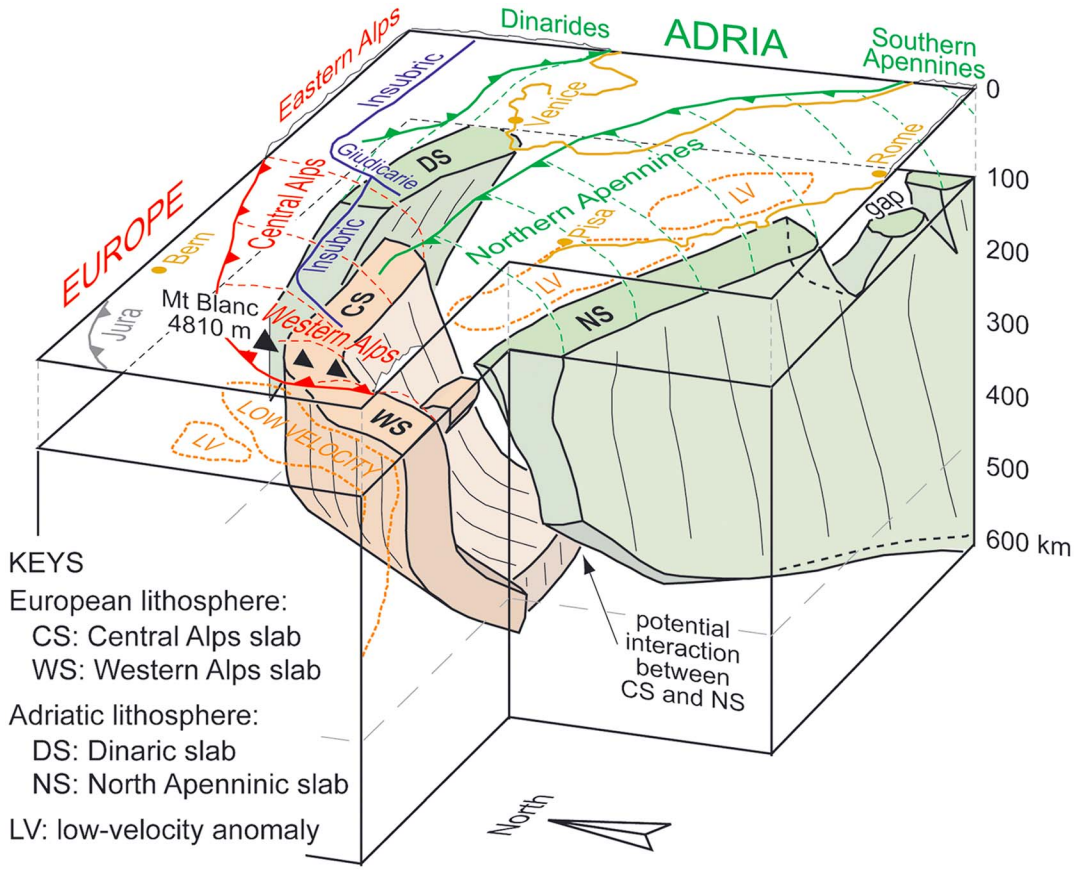

Figure 7. A 3-D schematic view of the European and Adriatic slabs as revealed by this tomography. The highest peaks of the Western Alps (black triangles), also including the Mont Blanc Massif, lay above a low-velocity anomaly detected in and beneath the European lithosphere.

cross-section A-A′, Figure 3a). The leakage of the weaker and thinner low-velocity anomalies simulating basins is also small. Such a weak smearing of crustal heterogeneities may be due to the following: (1) the very dense station coverage, in particular in the Western Alps with the CIFALPS experiment that crosses over three of the major crustal heterogeneities of the Alpine region (Southeast basin, Ivrea body, and Po Plain); (2) the finite-frequency tomography technique, as traveltimes computed with finite-frequency kernels are more sensitive to shallow heterogeneities than the classical ray-based tomography (see supporting information Figure S16); and (3) the inclusion of site (and event) terms in the inversion that accounts for baseline shifts between the relative residuals for different sites (and events) and probably part of the shallowest velocity heterogeneities [*Allen et al*., 2002]. The observed small leakage of crustal heterogeneities to mantle depth explains why the crustal corrections described in section 3.1 have a negligible contribution to our final velocity perturbation model, as displayed in the supporting information Figure S5.

This series of synthetic tests illustrates that wherever we input synthetic anomalies with size $>100\,\text{km} \times 100\,\text{km} \times 60\,\text{km}$ (in the horizontal and vertical directions) in the well-resolved area defined in Figures 2 and 3, they are reliably retrieved by our inversion. In the following section, we will only discuss features of larger size.

6. Discussion

This study reveals several new features of the upper mantle structure beneath the Alpine-Apenninic region. A 3-D schematic view summarizing these new features is shown in Figure 7. The major geodynamic implications are discussed below.

6.1. Along-Strike Slab Continuity and the Role of Inherited Structures

One of the most striking results of this study is the continuity of the Alpine slab from the Western Alps to the central Alps. Only its southern and eastern terminations appear discontinuous, suggesting the existence of lithospheric-scale transfer structures. The eastern termination of the Alpine slab matches at the surface with the Giudicarie Line (Figure 2a). The north dipping high-velocity anomaly to the east of the Giudicarie Line is consistent with the Dinaric structures mapped farther east [*Doglioni and Carminati*, 2002] and with an Adriatic polarity of subduction east of this fault [e.g., *Schmid et al*., 2004; *Vignaroli et al*., 2008; *Salimbeni et al*., 2013]. The Giudicarie Line represents a major Mesozoic paleogeographic boundary within the Adriatic Plate, inherited from Tethyan opening in the Jurassic, and separating during the whole Mesozoic the Lombardian basin (to the west) from the Trento high (to the east) [*Winterer and Bosellini*, 1981]. Moreover, the structural style in the South Alpine domain changes dramatically across the Giudicarie Line, from thick skinned to the west [*Zanchetta et al*., 2015] to thin skinned to the east [*Doglioni and Bosellini*, 1987], and this could be consistent with a retroside position of the South Alpine units to the west of the Giudicarie Line, compared to a proside position to the east. We propose that the Giudicarie Line may represent an inherited Mesozoic structure cutting across the Adriatic Tethyan margin, later reactivated as a tear fault [e.g., *Prosser*, 2000]. This would accommodate the opposite-dipping subductions beneath the central Alps and the Eastern Alps. The change in subduction polarity across the Giudicarie Line was already proposed by *Schmid et al*. [2004] based on the *Lippitsch et al*.'s [2003] *P* wave tomography, and it is further supported by the improved resolution of the Dinaric slab provided in this work. However, this does not exclude that European subduction took place at an earlier stage in the Eastern Alps until the final closure of the Alpine Tethys, to be resumed by Dinaric subduction only at a later stage (Figure 1b).

The absence of slab continuity between the Western Alps and the Northern Apennines is consistent with recent plate tectonic reconstructions of the central Mediterranean area [e.g., *Jolivet and Faccenna*, 2000; *Vignaroli et al*., 2008; *Dumont et al*., 2012; *Malusà et al*., 2015]. Starting from the end of the Oligocene, the Apenninic slab retreated eastward, while the Adriatic microplate still continued moving northward relative to Europe, leading to hard collision in the Alps (Figure 1b) [*Malusà et al*., 2016a]. This scenario requires $>$200 km left-lateral motion along lithospheric-scale transfer zones, possibly reactivating preexisting Mesozoic structures [e.g., *Malusà et al*., 2015, 2016b], in line with the observed slab discontinuity at depth along the complex Alps-Apennines transition zone. The interaction between the Western Alps slab and the northward shifting Apenninic slab before the onset of Neogene slab rollback may explain the occurrence of the enigmatic north dipping high-velocity anomaly (10 in Figure 3) observed along the Alps-Apennines transition zone. Such anomaly beneath the Ligurian Alps may represent a rotated lithospheric fragment previously belonging either to the Apenninic slab or to the Western Alps slab. In the interpretive model of Figure 7, we favor an Alpine origin for this lithospheric fragment. In fact, the Ligurian Alps were structured within the framework of Alpine subduction with no evidence of Apenninic tectonics [*Malusà et al*., 2015], and they underwent up to 90° counterclockwise rotation since the Oligocene, as documented by paleomagnetic data [e.g., *Maffione et al*., 2008]. A similar rotation, when experienced by an east dipping fragment of the Western Alps slab, would lead to a final north dipping attitude as observed in our tomographic images. This suggests that rotations detected within the Alpine orogenic wedge may have affected deeper levels of the Alpine subduction zone than previously inferred, along the transition zone between the Alps and the Apennines. Starting from the Neogene, however, the northward moving Apenninic slab may have started interacting with the central Alps slab (Figure 7), and such interaction may have controlled the location of the northern tip of the Ligurian-Provençal basin during Apenninic retreat [*Malusà et al*., 2016a].

6.2. Slab Steepness and Implications for (U)HP Metamorphism

Geophysical experiments carried out across the Alps consistently suggested a gently dipping European Moho beneath the Alpine orogenic wedge [e.g., *Lüschen et al*., 2004; *Zhao et al*., 2015], at least down to 50–75 km depth. Some of the recent geodynamic syntheses of the Mediterranean region [e.g., *Carminati and Doglioni*, 2012] have compared such a gentle dip with the much steeper dip inferred for the Apennines, emphasizing the possible role exerted by mantle flow in shaping subduction zones with different polarities. However, in the light of the very slow convergence rates documented at the Western Alps trench ($<$1 cm yr^{-1}), a gently dipping Alpine subduction would be hardly compatible with the very low

paleogeothermal gradients recorded by (U)HP metamorphic rocks during oceanic subduction [*Malusà et al*., 2015, Figure 11]. Our tomographic data show that the dip of the Alpine slab steepens to ~70° at depths >70 km. This implies relatively fast rock burial at (U)HP depth even for low convergence rates. This may have allowed attaining paleogeothermal gradients close to the forbidden zone (geothermal gradients $<5°C\,km^{-1}$, unexpected on Earth) during continental subduction, thus reconciling petrologic data with geophysical constraints.

By contrast, mechanisms leading to the exhumation of (U)HP rocks remain a debated issue. In the Alps, fast (U)HP rock exhumation has been reproduced by many of numerical models [e.g., *Yamato et al*., 2007, 2008; *Duretz et al*., 2011]. All these models not only predict slow exhumation across the upper crust, unlike observed in the geologic record, but also suggest slab break off after collision. In the Alpine region, the possibility of slab break off after (U)HP rock exhumation is ruled out by our new tomographic images. Exhumation models invoking divergence within the subduction zone, either due to slab rollback [e.g., *Brun and Faccenna*, 2008], hydration of the mantle wedge [*Gorczyk et al*., 2007], or due to the motion of the upper plate away from the trench [e.g., *Malusà et al*., 2011, 2015], are more consistent with the geologic record. They may explain the fast exhumation of (U)HP rocks in the lack of slab break off, as well as the gentle dip of the shallowest segment of the European slab imaged by recent geophysical investigations [*Zhao et al*., 2015].

6.3. Downdip Slab Continuity and Implications for Cenozoic Magmatism

Since *Davies and von Blanckenburg* [1995] first described the magmatic effects of oceanic-lithosphere detachment during continental collision, Cenozoic magmatism in the Alps has been explained by European slab break off [e.g., *Dal Piaz et al*., 2003]. The improved resolution of our tomography model sheds new light on this issue and attests to the downdip continuity of the European slab beneath the central Alps (Figure 7). Noteworthy, the amount of subducted lithosphere as seen in tomography cross sections (Figure 3) is fully consistent with the amount predicted by paleomagnetic and geological constraints [*Handy et al*., 2010; *Malusà et al*., 2015]. About 450 km subduction took place along the central Alps trench on a geological ground [*Malusà et al*., 2016a], and this is also the amount that can be inferred from the length of the high-velocity anomalies (1 in Figure 3). Moreover, the alpine volcanism in the Western Alps cannot be explained, to the south of the Cretaceous wedge, by slab break off of the European slab at 35 Ma, as it affects the proside foreland basin and not the upper plate (Adriatic) side of the orogen. Volcanism observed in Provence (PR in Figure 1a) is more likely related to flow and upwelling of hot mantle material beneath the European plate in relation to subduction of the nearby Apennine slab [*Jourdan et al*., 2013], which started retreating during the Neogene leading to the opening of the Ligurian-Provençal basin in the back-arc region [*Jolivet and Faccenna*, 2000] (see Figure 1b).

Even though our findings rule out slab break off as a viable explanation for Alpine magmatism, we cannot exclude that slab break off may have occurred at an earlier stage in the easternmost segments of the Adria-Europe plate boundary. As shown in Figure 1b, Dinaric subduction beneath the Eastern Alps was preceded by European subduction till the final closure of the Alpine Tethys. The onset of Dinaric subduction may thus have required the break off of the European slab in the Eastern Alps, but such break off is obviously unrelated to Alpine magmatism, as it took place, if any, in a different region of the Adria-Europe plate boundary zone.

In the Apennines, the timing and spatial distribution of orogenic magmatism is clearly linked to the progressive retreat of the Adriatic slab [e.g., *Lustrino et al*., 2011; *Carminati et al*., 2012]. Major compositional variations in magmatism are observed along strike [e.g., *Peccerillo and Frezzotti*, 2015], possibly controlled by slab tearing unraveled by major gaps in high-velocity anomalies [*Rosenbaum et al*., 2008]. Our tomography model confirms the existence of major gaps in the Adriatic slab at the boundary between the Northern and the Southern Apennines (Figures 2a and 7) as highlighted by *Lucente et al*. [1999], *Piromallo and Morelli* [2003], *Giacomuzzi et al*. [2011], and *Greve et al*. [2014]. These gaps match with major faults affecting the Apenninic wedge at the surface. They are observed in the 100 km depth slice but not documented at greater depth, and they define a slab structure consistent with the distribution of the main Plio-Quaternary Apenninic magmatic provinces [*Peccerillo and Frezzotti*, 2015]. Our tomography model also documents the along-strike continuity of the Adriatic slab in the Northern Apennines, suggesting that the role of slab tearing in this latter area is possibly overestimated [e.g., *Rosenbaum et al*., 2008].

6.4. Mantle Structure and Implications for Topography Development

Slab break off may exert a prominent control on topography development [e.g., *Platt and England*, 1994; *Davies and von Blanckenburg*, 1995]. This work, providing geophysical evidence that the European slab did not break off during the Paleogene, conclusively rules out this mechanism as a possible driver for Alpine topography.

Recent studies have underlined the importance of dynamic topography in the Mediterranean region [e.g., *Faccenna et al*., 2014, and references therein]. Our tomographic model shows that some of the highest peaks in the Alps, including the Mont Blanc and other external massifs, are located almost above a strong low-velocity anomaly observed at 100–250 km depth (8 in Figure 2a) and extending with lower amplitudes down to the mantle transition zone. In the Western Alps, the kinematic boundary conditions imposed by the present-day Adria-Europe relative plate motion lead to a stress regime partitioned between transtension in the accretionary wedge and transpression in the foreland [*Sue et al*., 1999; *Malusà et al*., 2009]. In addition, recent continuous GPS measurements show that the current horizontal shortening component is below the detection limit, while the vertical displacement is significant ($>2\,\mathrm{mm\,yr^{-1}}$) in areas of higher relief [*Serpelloni et al*., 2013; *Nocquet et al*., 2016]. Coupled uplift and seismic activity in the axial Western Alps cannot be simply explained by ongoing Adria-Europe convergence, or by postglacial rebound only [e.g., *Fox et al*., 2015], but appear to be governed by a combination of surface processes and dynamic topography.

Noteworthy, the uplift of the external massifs took place in the Neogene, well after the Cenozoic Alpine magmatism and the Eocene exhumation of (U)HP rocks [e.g., *Glotzbach et al*., 2011]. The location and depth range of the low-velocity anomaly detected beneath the external massifs (Figures 2a and 7) fits well with the orogen-parallel directions of fast shear wave velocities shown by *Barruol et al*. [2004] in the same area and interpreted as a response to the Neogene eastward retreat of the Apenninic slab [*Jolivet et al*., 2009]. Also, the timing of uplift and exhumation in the external massifs fits much better with progressive slab rollback of the Apenninic slab rather than with Alpine magmatism.

One possibility is that slab retreat has induced not only a suction effect of the asthenospheric mantle lying beneath the fore-arc side of the Alpine subduction, as proposed by previous work [*Barruol et al*., 2004; *Jolivet et al*., 2009], but also an asthenospheric upwelling at the boundary between the external and internal zones of the Western Alps. This may suggest a thermal origin for the low-velocity anomaly detected on the lower plate side of the Western Alps, which may explain the higher average elevation of this segment of the belt compared to other segments located farther east (i.e., the central Alps and Eastern Alps). However, further tests are required in order to confirm this hypothesis.

6.5. Magmatism, Uplift, and Exhumation: A Single Geodynamic Trigger?

Slab break off was first proposed in the Alpine region to simultaneously explain a range of different geologic observations, i.e., (U)HP exhumation, magmatism, and surface uplift [*von Blanckenburg and Davies*, 1995]. Even though slab break off in the central Alps and Western Alps is ruled out by our new tomographic images, other mechanisms may have a simultaneous impact on topography, magmatism, and exhumation along convergent plate boundaries.

Continental delamination [*Bird*, 1979] may cause isostatic uplift and an increased heat flow over a broad region above the lithospheric gap [*Göğüş and Pysklywec*, 2008], segregation of partial melts [*Elkins-Tanton*, 2007], reduced seismic velocity, and a negative Bouguer gravity anomaly. If the European Alps had experienced continental delamination, these effects should be observed on the Adriatic side of the orogen, which displays instead a positive Bouguer anomaly and high seismic velocities [*Zhao et al*., 2015]. A convective removal of the mantle lithosphere [*Houseman et al*., 1981] may also expose the thickened bottom of the European crust to asthenospheric temperatures, which would imply high temperatures beneath the Alpine roots. A hypothetical convective removal of the mantle lithosphere beneath the Alps would conflict with the very low paleogeothermal gradients experience by exhumed (U)HP rocks [*Malusà et al*., 2015, and references therein], and with the occurrence of anomalously deep earthquakes on the upper plate side of the Alpine orogen [*Eva et al*., 2015], which are supportive of still very low geothermal gradients on top of the Western Alps slab.

The general models proposed for subduction around the Pacific [e.g., *Uyeda and Kanamori*, 1979] and later applied to the Alps-Apennines system [e.g., *Doglioni et al*., 1999] are also inconsistent with the geophysical

evidence illustrated in this work. According to *Uyeda and Kanamori* [1979], an active margin should display either an elevated accretionary prism and a shallow dip slab, if the upper and lower plates are tightly coupled, or a steep dip slab and no uplift, if the upper and lower plates are decoupled. These predictions are not met in the European Alps, as they display both high elevation and a steeply dipping slab (Figure 3).

In the European Alps, (U)HP rock exhumation, magmatism, and topographic growth are sufficiently separated in time and space not to be necessarily linked to a single geodynamic trigger. The Eocene exhumation of (U)HP rocks in the Western Alps is possibly explained, e.g., by divergence between the upper plate and the accretionary wedge [*Malusà et al*., 2011, 2015]. Cenozoic Alpine magmatism, which is not spatially linked to (U)HP rock exhumation, may simply record the progressive subduction of oceanic and transitional lithosphere beneath the Adriatic Plate or, in SE France, return mantle flow related to the Apennine slab rollback. The Neogene topographic growth of the external massifs may be a far-field effect of this rollback of the Apenninic slab. None of the above mechanisms implies slab break off.

7. Conclusions

Our 3-D tomography model provides an improved image of the complex slab structure beneath the Alpine region and fundamental input for the analysis of Cenozoic magmatism, (U)HP metamorphism, and Alpine topography. Our data constrain the lateral continuity of the European slab from the Western Alps to the central Alps, as well as its downdip continuity, ruling out the hypothesis of slab break off as a viable mechanism for Cenozoic magmatism and topography development in the Alps. The dip of the European slab gets steeper in the upper mantle, reconciling geophysical constraints and petrologic evidence for very cold subduction. Another low-velocity anomaly, detected beneath the highest peaks of the Western Alps down to the mantle transition zone, may be supportive of mantle dynamic effects on Alpine topography, possibly induced by the Neogene rollback of the Apenninic slab. A NE dipping high-velocity anomaly consistent with Dinaric subduction is observed beneath the Eastern Alps, whereas the Adriatic slab shows a remarkable along-strike continuity in the Northern Apennines and major gaps at the boundary with the Southern Apennines that explain the compositional variability in orogenic magmatism. The Apenninic slab becomes short and near vertical close to the Alps-Apennines transition zone, where evidence for European slab fragmentation and rotation is possibly detected.

Our results show once again that high-quality traveltime data from dense seismic arrays and finite-frequency tomography may provide images of the mantle structure at odds with previous tomographies, in particular on the geometry of subducted slabs and possible slab break offs. This comment questions the validity of the numerous tomography interpretations made in other parts of the Alpine-Zagros-Himalaya orogenic belt where successive slab break offs have been proposed.

Acknowledgments

The seismic data of the CIFALPS experiment are archived at the data center of the Seismic Array Laboratory, Institute of Geology and Geophysics, Chinese Academy of Sciences, and at the data center of the French Seismologic and Geodetic Network RESIF (doi: 10.15778/RESIF.YP2012). The RESIF data center also hosts the data of the PYROPE experiment (doi: 10.15778/RESIF.X72010). We are most grateful to the operators of permanent broadband seismic arrays of European countries who make their data freely available through the EIDA (European Integrated Data Archive, http://www.orfeus-eu.org/eida/eida.html). Most of the permanent stations we used belong to networks CH (Switzerland Seismological Network), FR (RESIF and other broadband permanent networks in metropolitan France, doi: 10.15778/RESIF.FR), GR (German Regional Seismic Network), GU (Regional Seismic Network of North Western Italy, doi: 10.7914/SN/GU), IV (Italian National Seismic Network), MN (MEDNET Project), SL (Slovenia Seismic Network), and TH (Thüringer Seismisches Netz). The CIFALPS project is funded by the State Key Laboratory of Lithospheric Evolution, China, the National Natural Science Foundation of China (grant 41625016), the Youth Innovation Promotion Association CAS (2012055), and by a grant from Labex OSUG@2020 (Investissements d'avenir-ANR10 LABX56, France). We are grateful to Yinshuang Ai, Yumei He, Weiwei Xu, Guangbing Hou, and Ling Chen for their help, to Richard Allen for help with tomography codes, and to Wei Lin, Xianhua Li, Fuyuan Wu, Xiaofeng Liang, and Coffice 422 for constructive discussions. The manuscript benefited from insightful comments by Edi Kissling, Claudio Faccenna, Helle Pedersen, and two anonymous reviewers.

References

Allen, R. M., et al. (2002), Imaging the mantle beneath Iceland using integrated seismological techniques, *J. Geophys. Res.*, *107*(B12), 2325, doi:10.1029/2001JB000595.

Barruol, G., A. Deschamps, and O. Coutant (2004), Mapping upper mantle anisotropy beneath SE France by SKS splitting indicates Neogene asthenospheric flow induced by Apenninic slab roll-back and deflected by the deep Alpine roots, *Tectonophysics*, *394*(1), 125–138.

Bird, P. (1979), Continental delamination and the Colorado Plateau, *J. Geophys. Res.*, *84*, 7561–7571, doi:10.1029/JB084iB13p07561.

Brun, J. P., and C. Faccenna (2008), Exhumation of high-pressure rocks driven by slab rollback, *Earth Planet. Sci. Lett.*, *272*, 1–7.

Capitanio, F. A., G. Morra, S. Goes, R. F. Weinberg, and L. Moresi (2010), India-Asia convergence driven by the subduction of the Greater Indian continent, *Nat. Geosci.*, *3*(2), 136–139.

Carminati, E., and C. Doglioni (2012), Alps vs. Apennines: The paradigm of a tectonically asymmetric Earth, *Earth Sci. Rev.*, *112*, 67–96.

Carminati, E., M. Lustrino, and C. Doglioni (2012), Geodynamic evolution of the central and western Mediterranean: Tectonics vs. igneous petrology constraints, *Tectonophysics*, *579*, 173–192.

Chevrot, S. (2002), Optimal measurement of relative and absolute delay times by simulated annealing, *Geophys. J. Int.*, *151*, 164–171.

Chevrot, S., et al. (2014), High-resolution imaging of the Pyrenees and Massif Central from the data of the PYROPE and IBERARRAY portable array deployments, *J. Geophys. Res. Solid Earth*, *119*, 6399–6420, doi:10.1002/2014JB010953.

Closs, H., and Y. Labrouste (1963), *Recherches Séismologiques dans les Alpes Occidentales au Moyen des Grandes Explosions en 1956, 1958 et 1960*, *Année Géophys. Int., XII*, vol. 2, 241 pp., CNRS, Paris.

Dahlen, F. A., S. H. Hung, and G. Nolet (2000), Fréchet kernels for finite-frequency traveltimes—I. Theory, *Geophys. J. Int.*, *141*, 157–174.

Dal Piaz, G. V., A. Bistacchi, and M. Massironi (2003), Geological outline of the Alps, *Episodes*, *26*, 175–180.

Davies, J. H., and F. von Blanckenburg (1995), Slab breakoff: A model of lithosphere detachment and its test in the magmatism and deformation of collisional orogens, *Earth Planet. Sci. Lett.*, *129*, 85–102.

Dewey, J. F., M. L. Helman, E. Turco, D. H. W. Hutton, and S. D. Knott (1989), Kinematics of the western Mediterranean, in *Alpine Tectonics*, *Spec. Publ.*, vol. 45, edited by M. P. Coward, D. Dietrich, and R. G. Park, pp. 265–283, Geol. Soc., London.

Diehl, T., S. Husen, E. Kissling, and N. Deichmann (2009), High-resolution 3-D P-wave model of the Alpine crust, *Geophys. J. Int.*, *179*, 1133–1147.
Doglioni, C., and A. Bosellini (1987), Eoalpine and mesoalpine tectonics in the Southern Alps, *Geol. Rundsch.*, *76*, 735–754.
Doglioni, C., and E. Carminati (2002), The effects of four subductions in NE Italy, *Mem. Sci. Geol. Padova*, *54*, 1–4.
Doglioni, C., P. Harabaglia, S. Merlini, F. Mongelli, A. T. Peccerillo, and C. Piromallo (1999), Orogens and slabs vs. their direction of subduction, *Earth Sci. Rev.*, *45*(3), 167–208.
Dumont, T., S. Schwartz, S. Guillot, T. Simon-Labric, P. Tricart, and S. Jourdan (2012), Structural and sedimentary records of the Oligocene revolution in the Western Alpine arc, *J. Geodyn.*, doi:10.1016/j.jog.2011.11.006.
Duretz, T., T. V. Gerya, and D. A. May (2011), Numerical modelling of spontaneous slab breakoff and subsequent topographic response, *Tectonophysics*, *502*, 244–256.
Elkins-Tanton, L. T. (2007), Continental magmatism, volatile recycling, and a heterogeneous mantle caused by lithospheric gravitational instabilities, *J. Geophys. Res.*, *112*, B03405, doi:10.1029/2005JB004072.
Eva, E., M. G. Malusà, and S. Solarino (2015), A seismotectonic picture of the inner southern Western Alps based on the analysis of anomalously deep earthquakes, *Tectonophysics*, *661*, 190–199, doi:10.1016/j.tecto.2015.08.040.
Faccenna, C., et al. (2014), Mantle dynamics in the Mediterranean, *Rev. Geophys.*, *52*, 283–332, doi:10.1002/2013RG000444.
Fox, M., F. Herman, E. Kissling, and S. D. Willett (2015), Rapid exhumation in the Western Alps driven by slab detachment and glacial erosion, *Geology*, *43*, 379–382.
Giacomuzzi, G., C. Chiarabba, and P. De Gori (2011), Linking the Alps and Apennines subduction systems: New constraints revealed by high-resolution teleseismic tomography, *Earth Planet. Sci. Lett.*, *301*, 531–543.
Glotzbach, C., P. A. Van Der Beek, and C. Spiegel (2011), Episodic exhumation and relief growth in the Mont Blanc massif, Western Alps from numerical modelling of thermochronology data, *Earth Planet. Sci. Lett.*, *304*(3), 417–430.
Göğüş, O. H., and R. N. Pysklywec (2008), Near-surface diagnostics of dripping or delaminating lithosphere, *J. Geophys. Res.*, *113*, B11404, doi:10.1029/2007JB005123.
Gorczyk, W., S. Guillot, T. V. Gerya, and K. H. Hattori (2007), Asthenospheric upwelling, oceanic slab retreat and exhumation of UHP mantle rocks: Insights from Greater Antilles, *Geophys. Res. Lett.*, *34*, L21309, doi:10.1029/2007GL031059.
Greve, S., H. Paulssen, S. Goes, and M. van Bergen (2014), Shear-velocity structure of the Tyrrhenian Sea: Tectonics, volcanism and mantle (de) hydration of a back-arc basin, *Earth Planet. Sci. Lett.*, *400*, 45–53.
Guillot, S., K. Hattori, P. Agard, S. Schwartz, and O. Vidal (2009), *Exhumation Processes in Oceanic and Continental Subduction Contexts: A Review*, Springer, Berlin.
Hafkenscheid, E., M. J. R. Wortel, and W. Spakman (2006), Subduction history of the Tethyan region derived from seismic tomography and tectonic reconstructions, *J. Geophys. Res.*, *111*, B08401, doi:10.1029/2005JB003791.
Handy, M. R., S. M. Schmid, R. Bousquet, E. Kissling, and D. Bernoulli (2010), Reconciling plate-tectonic reconstructions of Alpine Tethys with the geological-geophysical record of spreading and subduction in the Alps, *Earth Sci. Rev.*, *102*, 121–158.
Houseman, G. A., D. P. McKenzie, and P. Molnar (1981), Convective instability of a thickened boundary layer and its relevance for the thermal evolution of continental convergent belts, *J. Geophys. Res.*, *86*, 6115–6132, doi:10.1029/JB086iB07p06115.
Hung, S., F. A. Dahlen, and G. Nolet (2000), Fréchet kernels for finite-frequency traveltimes—II. Examples, *Geophys. J. Int.*, *141*, 175–203.
Hung, S., Y. Shen, and L. Chiao (2004), Imaging seismic velocity structure beneath the Iceland hot spot: A finite frequency approach, *J. Geophys. Res.*, *109*, B08305, doi:10.1029/2003JB002889.
Jolivet, L., and C. Faccenna (2000), Mediterranean extension and the Africa-Eurasia collision, *Tectonics*, *19*, 1095–1106, doi:10.1029/2000TC900018.
Jolivet, L., C. Faccenna, and C. Piromallo (2009), From mantle to crust: Stretching the Mediterranean, *Earth Planet. Sci. Lett.*, *285*(1), 198–209.
Jourdan, S., M. Bernet, P. Tricart, E. Hardwick, J. L. Paquette, S. Guillot, T. Dumont, and S. Schwartz (2013), Short-lived fast erosional exhumation of the internal Western Alps during the late Early Oligocene: Constraints from geo-thermochronology of pro- and retro-side foreland basin sediments, *Lithosphere*, *5*, 211–225, doi:10.1130/L243.1.
Kissling, E. (1993), Deep structure of the Alps—What do we really know?, *Phys. Earth Planet. Inter.*, *79*, 87–112.
Kissling, E., S. M. Schmid, R. Lippitsch, J. Ansorge, and B. Fügenschuh (2006), Lithosphere structure and tectonic evolution of the Alpine arc: New evidence from high-resolution teleseismic tomography, *Geol. Soc. London Mem.*, *32*, 129–145.
Lippitsch, R., E. Kissling, and J. Ansorge (2003), Upper mantle structure beneath the Alpine orogen from high-resolution teleseismic tomography, *J. Geophys. Res.*, *108*(B8), 2376, doi:10.1029/2002JB002016.
Lucente, F. P., C. Chiarabba, G. B. Cimini, and D. Giardini (1999), Tomographic constraints on the geodynamic evolution of the Italian region, *J. Geophys. Res.*, *104*, 20,307–20,327, doi:10.1029/1999JB900147.
Lüschen, E., B. Lammerer, H. Gebrande, K. Millahn, R. Nicolich, and TRANSALP Working Group (2004), Orogenic structure of the Eastern Alps, Europe, from TRANSALP deep seismic profiling, *Tectonophysics*, *388*, 85–102.
Lustrino, M., S. Duggen, and C. L. Rosenberg (2011), The Central-Western Mediterranean: Anomalous igneous activity in an anomalous collisional tectonic setting, *Earth Sci. Rev.*, *104*, 1–40.
Maffione, M., F. Speranza, C. Faccenna, A. Cascella, G. Vignaroli, and L. Sagnotti (2008), A synchronous Alpine and Corsica-Sardinia rotation, *J. Geophys. Res.*, *113*, B03104, doi:10.1029/2007JB005214.
Malusà, M. G., R. Polino, and M. Zattin (2009), Strain partitioning in the axial NW Alps since the Oligocene, *Tectonics*, *28*, TC3005, doi:10.1029/2008TC002370.
Malusà, M. G., C. Faccenna, E. Garzanti, and R. Polino (2011), Divergence in subduction zones and exhumation of high pressure rocks (Eocene Western Alps), *Earth Planet. Sci. Lett.*, *310*(1), 21–32.
Malusà, M. G., C. Faccenna, S. L. Baldwin, P. G. Fitzgerald, F. Rossetti, M. L. Balestrieri, M. Danišík, A. Ellero, G. Ottria, and C. Piromallo (2015), Contrasting styles of (U)HP rock exhumation along the Cenozoic Adria-Europe plate boundary (Western Alps, Calabria, Corsica), *Geochem. Geophys. Geosyst.*, *16*, 1786–1824, doi:10.1002/2015GC005767.
Malusà, M. G., O. A. Anfinson, L. N. Dafov, and D. F. Stockli (2016a), Tracking Adria indentation beneath the Alps by detrital zircon U-Pb geochronology: Implications for the Oligocene–Miocene dynamics of the Adriatic microplate, *Geology*, *44*(2), 155–158.
Malusà, M. G., M. Danišík, and J. Kuhlemann (2016b), Tracking the Adriatic-slab travel beneath the Tethyan margin of Corsica-Sardinia by low-temperature thermochronometry, *Gondwana Res.*, doi:10.1016/j.gr.2014.12.011.
Maupin, V., and M. L. Kolstrup (2015), Insights in *P*- and *S*-wave relative traveltime tomography from analyzing finite-frequency Fréchet kernels, *Geophys. J. Int.*, *202*, 1581–1598, doi:10.1093/gji/ggv239.
Molinari, I., and A. Morelli (2011), EPcrust: A reference crustal model for the European Plate, *Geophys. J. Int.*, *185*, 352–364, doi:10.1111/j.1365-246X.2011.04940.x.
Nocquet, J. M., et al. (2016), Present-day uplift of the western Alps, *Sci. Rep.*, *6*, 28404, doi:10.1038/srep28404.

Paige, C. C., and M. A. Saunders (1982), LSQR: An algorithm for sparse linear equations and sparse least squares, *Trans. Math. Software*, *8*, 43–71.
Peccerillo, A., and M. L. Frezzotti (2015), Magmatism, mantle evolution and geodynamics at the converging plate margins of Italy, *J. Geol. Soc. London*, doi:10.1144/jgs2014-085.
Piromallo, C., and C. Faccenna (2004), How deep can we find the traces of Alpine subduction?, *Geophys. Res. Lett.*, *31*, L06605, doi:10.1029/2003GL019288.
Piromallo, C., and A. Morelli (2003), *P* wave tomography of the mantle under the Alpine-Mediterranean area, *J. Geophys. Res.*, *108*(B2), 2065, doi:10.1029/2002JB001757.
Platt, J. P., and P. C. England (1994), Convective removal of lithosphere beneath mountain belts: Thermal and mechanical consequences, *Am. J. Sci.*, *294*, 307–336.
Prosser, G. (2000), The development of the North Giudicarie fault zone (Insubric line, Northern Italy), *J. Geodyn.*, *30*, 229–250.
Replumaz, A., H. Kárason, R. D. van der Hilst, J. Besse, and P. Tapponnier (2004), 4-D evolution of SE Asia's mantle from geological reconstructions and seismic tomography, *Earth Planet. Sci. Lett.*, *221*, 103–115.
Rosenbaum, G., M. Gasparon, F. P. Lucente, A. Peccerillo, and M. S. Miller (2008), Kinematics of slab tear faults during subduction segmentation and implications for Italian magmatism, *Tectonics*, *27*, TC2008, doi:10.1029/2007TC002143.
Rubatto, D., and J. Hermann (2001), Exhumation as fast as subduction?, *Geology*, *29*, 3–6.
Salimbeni, S., S. Pondrelli, and L. Margheriti (2013), Hints on the deformation penetration induced by subductions and collision processes: Seismic anisotropy beneath the Adria region (Central Mediterranean), *J. Geophys. Res. Solid Earth*, *118*, 5814–5826, doi:10.1002/2013JB010253.
Schmid, S. M., B. Fügenschuh, E. Kissling, and R. Schuster (2004), Tectonic map and overall architecture of the Alpine orogen, *Eclogae Geol. Helv.*, *97*(1), 93–117.
Serpelloni, E., C. Faccenna, G. Spada, D. Dong, and S. D. P. Williams (2013), Vertical GPS ground motion rates in the Euro-Mediterranean region: New evidence of velocity gradients at different spatial scales along the Nubia-Eurasia plate boundary, *J. Geophys. Res. Solid Earth*, *118*, 6003–6024, doi:10.1002/2013JB010102.
Solarino, S., D. Spallarossa, S. Parolai, M. Cattaneo, and C. Eva (1996), Litho-asthenospheric structures of northern Italy as inferred from teleseismic P-wave tomography, *Tectonophysics*, *260*, 271–289.
Spada, M., I. Bianchi, E. Kissling, N. Piana Agostinetti, and S. Wiemer (2013), Combining controlled-source seismology and receiver function information to derive 3-D Moho topography for Italy, *Geophys. J. Int.*, *194*, 1050–1068, doi:10.1093/gji/ggt148.
Spakman, W., and R. Wortel (2004), A tomographic view on western Mediterranean geodynamics, in *The TRANSMED Atlas: The Mediterranean Region From Crust to Mantle*, pp. 31–52, Springer, Berlin.
Spakman, W., S. van der Lee, and R. van der Hilst (1993), Travel-time tomography of the European-Mediterranean mantle down to 1400 km, *Phys. Earth Planet. Inter.*, *79*, 3–74.
Sue, C., F. Thouvenot, J. Fréchet, and P. Tricart (1999), Widespread extension in the core of the Western Alps revealed by earthquake analysis, *J. Geophys. Res.*, *104*, 25,611–25,622, doi:10.1029/1999JB900249.
Uyeda, S., and H. Kanamori (1979), Back-arc opening and the mode of subduction, *J. Geophys. Res.*, *84*, 1049–1061, doi:10.1029/JB084iB03p01049.
Vandecar, J. C., and R. S. Crosson (1990), Determination of teleseismic relative phase arrival times using multi-channel cross-correlation and least squares, *Bull. Seismol. Soc. Am.*, *80*, 150–169.
Vignaroli, G., C. Faccenna, L. Jolivet, C. Piromallo, and F. Rossetti (2008), Subduction polarity reversal at the junction between the Western Alps and the Northern Apennines, Italy, *Tectonophysics*, *450*(1), 34–50.
von Blanckenburg, F., and J. H. Davies (1995), Slab breakoff: A model for syncollisional magmatism and tectonics in the Alps, *Tectonics*, *14*, 120–131, doi:10.1029/94TC02051.
Waldhauser, F., R. Lippitsch, E. Kissling, and J. Ansorge (2002), High-resolution teleseismic tomography of upper-mantle structure using an a priori three-dimensional crustal model, *Geophys. J. Int.*, *150*, 403–414.
Winterer, E. L., and A. Bosellini (1981), Subsidence and sedimentation on a Jurassic passive continental margin, Southern Alps, Italy, *Am. Assoc. Pet. Geol. Bull.*, *65*, 394–421.
Wortel, M. J. R., and W. Spakman (2000), Subduction and slab detachment in the Mediterranean-Carpathian region, *Science*, *290*(5498), 1910–1917.
Yamato, P., P. Agard, E. Burov, L. Le Pourhiet, L. Jolivet, and C. Tiberi (2007), Burial and exhumation in a subduction wedge: Mutual constraints from thermomechanical modeling and natural P-T-t data (Schistes Lustrés, western Alps), *J. Geophys. Res.*, *112*, B07410, doi:10.1029/2006JB004441.
Yamato, P., E. Burov, P. Agard, L. Le Pourhiet, and L. Jolivet (2008), HP-UHP exhumation during slow continental subduction: Self-consistent thermodynamically and thermomechanically coupled model with application to the Western Alps, *Earth Planet. Sci. Lett.*, *271*(1), 63–74.
Zanchetta, S., M. G. Malusà, and A. M. Zanchi (2015), Precollisional development and Cenozoic evolution of the Southalpine retrobelt (European Alps), *Lithosphere*, *7*, 662–681, doi:10.1130/L466.1.
Zhao, L., et al. (2015), First seismic evidence for continental subduction beneath the Western Alps, *Geology*, *43*, 815–818.